Oxygen Intercalation under Graphene on Ir(111): Energetics, Kinetics, and the Role of Graphene Edges

Elin Grånäs,[†] Jan Knudsen,[†] Ulrike A. Schröder,[‡] Timm Gerber,[‡] Carsten Busse,[‡] Mohammad A. Arman,[†] Karina Schulte,[§] Jesper N. Andersen,[†,§] and Thomas Michely[‡,*]

[†]Division of Synchrotron Radiation Research and [§]MAX IV Laboratory, Lund University, Box 118, 221 00 Lund, Sweden and [‡]II. Physikalisches Institut, Universität zu Köln, 50937 Köln, Zülpicher Strasse 77, Germany

ABSTRACT Using X-ray photoemission spectroscopy (XPS) and scanning tunneling microscopy (STM) we resolve the temperature-, time-, and flake size-dependent intercalation phases of oxygen underneath graphene on Ir(111) formed upon exposure to molecular oxygen. Through the applied pressure of molecular oxygen the atomic oxygen created on the bare Ir terraces is driven underneath graphene flakes. The importance of substrate steps and of the unbinding of graphene flake edges from the substrate for the intercalation is identified. With the use of CO titration to selectively remove oxygen from the bare Ir terraces the energetics of intercalation is uncovered. Cluster decoration techniques are used as an efficient tool to visualize intercalation processes in real space.

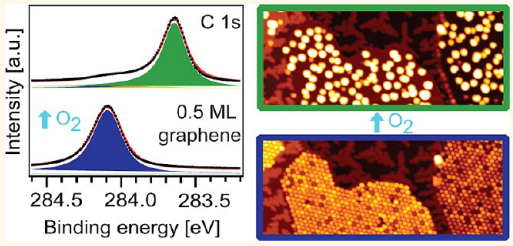

KEYWORDS: X-ray photoemission spectroscopy · scanning tunneling microscopy · graphene · oxygen intercalation · Ir(111)

Intercalation of atoms or molecules in between an epitaxial graphene layer and its substrate has become an intensively studied topic. This strong interest is driven by the unique opportunities to modify its binding, to decouple graphene from its substrate,[1−9] to perform or suppress chemistry under graphene,[10,11] to enable exfoliation,[12] or to bestow it with entirely new properties mediated by the intercalation layer.

For graphene flakes on Ru(0001)—strongly bound to the substrate—oxygen intercalation upon exposure to molecular oxygen has been intensely studied by microscopy and spectroscopy.[10,11,13] For temperatures around 600 K and below, where oxygen etching is absent, intercalation proceeds from the edges of graphene flakes toward the interior with a phase boundary separating intercalated and nonintercalated graphene areas.[10,11] The saturated intercalation phase is assigned to a p(2 × 1)-O structure sandwiched between Ru(0001) and graphene.[5,10] During intercalation, Starodub *et al.*[11] observed two well-defined fronts in low energy electron microscopy (LEEM), which they speculate to be linked to O-phases below graphene with low and high O concentrations. From their LEEM movies, Sutter *et al.*[10] concluded that the rate limiting step for oxygen intercalation is the decoupling of graphene from the substrate at the reaction front.

For graphene on Ir(111), intercalation of oxygen upon exposure to molecular oxygen has only been studied in the context of graphene etching by Starodub *et al.*[11] On the basis of their observations at elevated temperatures, the authors concluded that direct attack of graphene by intercalated oxygen is the main route for graphene etching on Ir(111).

In addition, two independent studies by Vinogradov *et al.*[14] and Larciprete *et al.*[15] used reactive O radicals to study the oxidation of graphene resting on Ir(111). Both studies concluded that epoxy groups (C−O−C) are formed, but they disagreed about the existence and XPS-fingerprints of intercalated oxygen.

Here, for graphene on Ir(111), weakly bound to the substrate, we investigate the intercalation of oxygen underneath graphene in a temperature range below the onset of graphene etching. Moreover, we take advantage of our ability to tailor the morphology of graphene on Ir(111) in a controlled way. We prepare a perfectly closed graphene layer as a reference and investigate intercalation underneath graphene flakes with circle equivalent (CE) diameters of the order of 10−100 nm, two to three orders of magnitude less than the size of the flakes investigated in the LEEM

* Address correspondence to michely@ph2.uni-koeln.de.

Received for review August 6, 2012 and accepted October 5, 2012.

Published online October 05, 2012
10.1021/nn303548z

studies mentioned above.[10,11] The graphene fabricated for our experiments is virtually defect-free displaying the characteristic (9.32 × 9.32) incommensurate moiré superstructure.[16,17] Such phase pure graphene, without misoriented sheets[18,19], is essential for our studies, as we apply XPS as a laterally averaging technique to identify chemical processes. At the temperatures, pressures, and exposures investigated, oxygen does not dissolve into the bulk of Ir and therefore the system under concern is a true two-dimensional (2D) system.[20]

Armed with such a well-defined system, the chemical sensitivity of XPS, and the detailed atomic scale view of STM we are able to answer the following fundamental questions: What are the fingerprints of intercalation in XPS and STM? Are there several distinguishable intercalation phases and what are their characteristics? What is the rate limiting step for oxygen intercalation and how does it depend on flake morphology? Is the intercalation probability a function of graphene flake size? Is there an effect of substrate steps on intercalation? Is there an energy gain associated with the intercalation of oxygen? How does intercalation depend on an applied molecular oxygen pressure?

Using *in situ* XPS and STM during intercalation as well as Pt-cluster decoration techniques we develop a complete picture of the kinetics and energetics of oxygen intercalation under graphene on Ir(111). The kinetic principles and the importance of graphene delamination to understand the energetics of intercalation are believed to hold for many epitaxial graphene systems.

RESULTS AND DISCUSSION

In the first part of the manuscript we determine the XPS fingerprints of intercalation under graphene flakes with CE diameters of 10−100 nm. In Figure 1 we display the C 1s spectra of a 0.5 ± 0.1 ML graphene/Ir(111) surface before (lowest spectra) and after oxygen exposure at stepwise increasing temperatures.

Before oxygen exposure, the 0.5 ML spectrum can be fitted by a single component (C_{Ir}) at 284.09 ± 0.05 eV with identical Gaussian and Lorentzian full width at half-maximum (GFWHM and LFWHM) of 0.16 eV. This width is in agreement with our earlier studies, where we also established that the height modulation of the graphene layer can be correlated with a 140 meV modulation of the C 1s core level shift (CLS).[21]

For the 0.5 ML graphene flakes oxygen exposure up to 355 K leads to the development of a low binding energy shoulder, whereas higher temperatures result in a new C 1s component (C_3) positioned at 283.64 ± 0.02 eV, a shift of −0.45 ± 0.02 eV compared to the C_{Ir} component of pristine graphene. The two intermediate components C_1 and C_2 (shifted −0.17 ± 0.03 eV, respectively −0.34 ± 0.03 eV compared to C_{Ir}), also

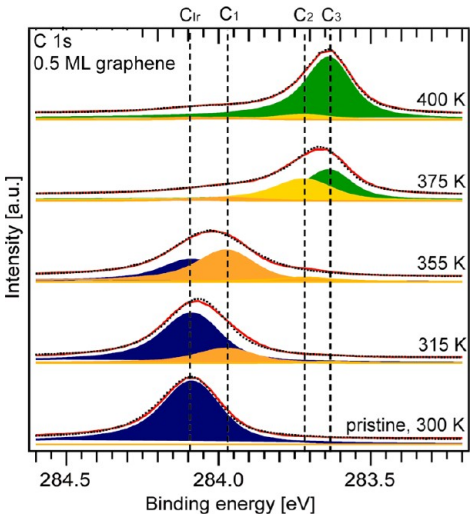

Figure 1. XP-spectra of the C 1s region of 0.5 ML graphene/Ir(111). The sample was exposed to 750 L of O_2 at stepwise increasing temperature, as indicated in the figure. The pristine graphene film is shown in the lowest spectra. The experimental spectra are shown as black dots, the fits as solid lines, and the filled curves represent the components of each fit. The dashed lines are the fitted binding energy positions.

seen in Figure 1, were introduced since it is impossible to fit the C 1s spectra after oxygen exposure with only one C_{Ir} and one C_3 component. They both have the same width parameters as the C_{Ir} component. We note that binding energies and estimated error bars of the C_{Ir}, C_1, C_2, and C_3 components are based on a number of experiments. The assignment of the C_1 and C_2 components will be discussed below, after we analyzed the nature of the C_3 component. Following oxygen exposure at 400 K the C_3 component fully dominates the spectrum. The GFWHM of the new C_3 component is 0.11 eV and thus reduced 31% with respect to the C_{Ir} component of pristine graphene. Since the GFWHM of graphene is coupled to the height modulation of the film above the Ir(111) surface,[21] the decreased width suggests that the height modulation is reduced upon oxygen exposure at 400 K. The peak area of the C_3 component after oxygen exposure at 400 K is, within the error limits, identical to the peak area of the C_{Ir} component of the pristine graphene. Therefore, we conclude that etching of graphene has not yet started. Since O_2 dosing at 400 K leads to one single C 1s component, with a −0.45 eV CLS, we conclude that all C-atoms are chemically equivalent after oxygen exposure. Further, the identical intensity of pristine and oxygen exposed graphene and the decreased C 1s width after oxygen exposure suggest that the chemically equivalent C-atoms are located in an intact graphene film. Finally, it is obvious from Figure 1 that the development of the C_3 component is strongly temperature dependent and only fully developed at 400 K.

For a perfectly closed 1 ML graphene layer with no bare Ir, we find after oxygen exposure at temperatures

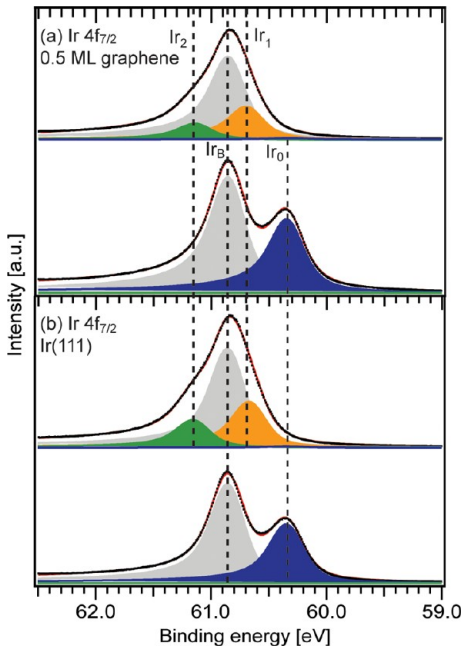

Figure 2. Ir $4f_{7/2}$ spectrum of (a) 0.5 ML graphene/Ir(111) and (b) clean Ir(111). The lower spectra of panels a and b are taken before and the upper ones after exposure to 750 L of O_2. The 0.5 ML graphene was exposed at 400 K and the Ir(111) at room temperature. The experimental spectra are shown as black dots, the fits as solid lines, and the filled curves represent the components of the fit.

up to 700 K that the peak position, FWHM, and peak area remains unchanged (see Figure S1 in the Supporting Information). This holds even for oxygen pressures up to 10^{-3} mbar. After oxygen exposure at 700 K STM imaging confirms the structural and chemical integrity of the 1 ML graphene, being indistinguishable from pristine graphene (see Figure S2 in the Supporting Information). However, for a graphene layer with small pinholes always a C_3 component arises well below 700 K. Thus, the C_3 component as well as the C_2 and C_1 components are unique for a situation where at least small patches of Ir(111) are uncovered by graphene.

In earlier XPS studies of atomic oxygen adsorption onto graphene/Ir(111)[14,15] epoxy groups were identified and assigned to a C 1s component with a binding energy of 284.6−285.9 eV. The absence of any peak in this energy interval shows that no epoxy groups are formed when monolayer and submonolayer graphene films are exposed to molecular oxygen. The C_3 component we observe at 283.64 eV must therefore originate from another oxygen related carbon species on the surface.

Figure 2a,b show the Ir $4f_{7/2}$ core level spectra of Ir(111) supporting 0.5 ML graphene and clean Ir(111), before (lower) and after oxygen exposure at 400 K (upper). Initially both spectra consist of one Ir $4f_{7/2}$ bulk component (Ir_B) at 60.81 eV and one surface component (Ir_0) shifted −0.50 eV with a GFWHM of 0.25 eV and a LFWHM of 0.21 eV consistent with the data of Ng *et al.*[22] Upon oxygen exposure of the 0.5 ML film the iridium surface component, Ir_0, decreases to 3% of its initial value. Therefore, 97% of all Ir(111) surface atoms, with and without graphene atop, are affected by the oxygen dosing. As the Ir_0 component disappears two new components appear, one at lower binding energy (−0.19 eV) compared to bulk, called Ir_1, and one at higher binding energy (+0.30 eV), called Ir_2. The CLS of the two new oxygen induced features Ir_1 and Ir_2 in Figure 2a are identical with those measured for oxygen on Ir(111) upon room temperature oxygen exposure, seen in Figure 2b. Previous studies[23,24] have shown that exposure of molecular oxygen onto Ir(111) leads to dissociation and formation of rotated microdomains of a defective p(2 × 1) structure with oxygen atoms adsorbed in the 3-fold hollow sites. In a p(2 × 1) structure Ir surface atoms are bound either to one oxygen atom or to two oxygen atoms. This gives rise to the two components, Ir_1, and Ir_2.[24] We therefore tentatively conclude that oxygen intercalated the graphene flakes with a defective p(2 × 1) structure—the same structure as formed on bare Ir(111)—and substantiate this conclusion in the following by a careful analysis of the Ir components for situations with different graphene coverages.

By normalizing the intensity of the Ir_0, Ir_1, and Ir_2 components in Figure 2a to the total surface intensity, the coverage of the respective types of Ir surface atoms can be calculated to be: $\theta_0 = 0.03$ ML, $\theta_1 = 0.70$ ML, and $\theta_2 = 0.27$ ML. Since each oxygen atom adsorbed forms three bonds with the Ir surface atoms, the oxygen coverage θ_{Ox} is simply one-third of the sum of the coverages of surface atoms, each multiplied by their number of bonds to oxygen atoms: $\theta_{Ox} = {}^1/_3 \cdot (0 \cdot \theta_0 + 1 \cdot \theta_1 + 2 \cdot \theta_2) = 0.41 \pm 0.02$ ML. In a similar experiment for a graphene coverage of 0.95 ML exposed to 750 L O_2 at 460 K we get ${}^1/_3 \cdot (0 \cdot 0.00$ ML $+ 1 \cdot 0.71$ ML $+ 2 \cdot 0.29$ ML$) = 0.43 \pm 0.02$ ML (see Figure S3 in the Supporting Information). Note, for the 0.95 ML coverage photoelectron attenuation by graphene atop is not an issue as we compare relative intensities of Ir atoms nearly all underneath graphene. The coexistence of Ir_1 and Ir_2 atoms on O-saturated samples with 0.5 and 0.95 ML graphene coverage is unambiguous evidence for a defective p(2 × 1)-O structure. These components only appear when oxygen atoms are placed with single and double Ir−Ir spacing to Ir(111) 3-fold hollow sites. Further, the existence of large areas of p(2 × 2)-O structure is ruled out by the complete disappearance of the Ir_0 component, as it would give rise to a significant amount of Ir_0 atoms [25% for 1 ML of p(2 × 2)-O]. For reference, curve fitting of the oxygen exposed Ir(111) surface without graphene [Figure 2b] reveals the following coverages: $\theta_0 = 0.01$ ML, $\theta_1 = 0.62$ ML, and $\theta_2 = 0.37$ ML which results in $\theta_{Ox} = 0.45 \pm 0.02$ ML. Thus, within the error limits we obtain the identical oxygen coverages, independent of graphene coverage.

Bianchi *et al.*[24] found a slightly lower saturation coverage of $\theta_{Ox} = 0.38$ ML at 80 K on Ir(111). In contrast

to our method this saturation coverage was found by extrapolating the Ir_0 curve to zero coverage and fixing the corresponding O 1s signal to $^1/_3$ ML. The intensity of the Ir_0, Ir_1, and Ir_2 components at saturation coverage are, however, also reported in the work of Bianchi *et al*. On the basis of their values and our method for calculating the oxygen coverage we obtain $^1/_3 \cdot (0 \cdot 0.06$ ML $+ 1 \cdot 0.58$ ML $+ 2 \cdot 0.37$ ML) = 0.44 ML, within the error limits identical to our value.

The fact that oxygen exposure at 400 K (0.5 ML)−460 K (0.95 ML) leads to chemically equivalent C-atoms, with a CLS of −0.45 eV, a disappearance of the Ir_0 component on graphene covered Ir(111), within the limits of error, identical oxygen coverages and binding energy positions Ir_1 and Ir_2 irrespective of the graphene coverage up to 0.95 ML can only be explained if oxygen intercalates the graphene flakes at these temperatures. On the bais of these observations we assign the C_3 component in the C 1s spectrum to graphene detached from the Ir(111) surface by an intercalated, defective, p(2 × 1)-O layer. Further evidence for the structural assignment of the C_3 component comes from the low energy electron diffraction (LEED) image of the O-intercalated 0.95 ML graphene that displays clearly visible half order diffraction spots with respect to the first order Ir(111) ones (see Figure S4 in the Supporting Information). In addition, we note that a negative C 1s CLS upon oxygen intercalation both is consistent with less strongly bound graphene and a net hole doping of the graphene sheet by the oxygen (see the Supporting Information for a longer discussion of the origin of the C 1s CLS for the C_3 component).

Finally, our assignment is supported by the O 1s core level spectra of fully O-intercalated graphene and O-covered Ir(111), which reveals an identical O 1s peak position at 529.9 eV (see Figure S5 in the Supporting Information). For a perfectly closed 1 ML graphene layer no oxygen signal was observed, neither before nor after oxygen exposure at a temperature up to 700 K. Since the binding energy of the O 1s peak originating from the p(2 × 1)-O structure on Ir(111) is independent of whether or not a graphene flake is located above we conclude that the oxygen-atoms bind to the Ir substrate and if at all, only interact weakly with graphene. We did not observe any O 1s features at 531.1 eV (epoxy groups) and 532.4 eV (ethers) in contrast to the studies of atomic oxygen on graphene/Ir(111),[14,15] further confirming that oxygen is not adsorbed on the graphene, but rather on the metal surface.

After assigning the C_3 component we continue with the analysis of the C_1 component that dominates the C 1s spectrum taken after oxygen exposure at 355 K (see Figure 1). Curve fitting of this C 1s spectrum reveals the following relative intensities: C_{Ir} (43%), C_1 (52%), and C_2 (5%). From fitting the corresponding Ir $4f_{7/2}$ spectrum ($\theta_0 = 0.39$ ML $\theta_1 = 0.51$ ML, $\theta_2 = 0.10$ ML) we find a total oxygen coverage of 0.24 ± 0.02 ML. As half of the surface area is bare Ir with a saturation coverage of 0.45 ML determined earlier, 0.24 ML − 0.5 × 0.45 ML = 0.015 ML of the total oxygen coverage is left for intercalation under the graphene flakes. As the flakes cover only half the surface area, the local coverage under the graphene flakes is twice as large, that is, amounts to 0.03 ML. Note that we subtract here large numbers with substantial errors resulting in an uncertainty of the order of 100% for the oxygen concentration underneath the graphene flakes. Nevertheless, on the basis of this estimate we assign the C_1 component in Figure 1 to a dilute oxygen lattice gas. Referring to Figure 1 it is evident that the C_1 component develops at temperatures between 315 and 355 K. We explain this observation by the onset of mobility of the O-adatoms within this temperature interval.

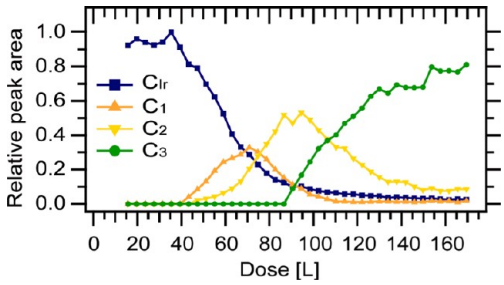

Figure 3. The time evolution of the components of the C 1s spectra measured in real time as 0.5 ML graphene on Ir(111) is exposed to 1 × 10^{-7} mbar, at 380 K. The spectra were fitted using the same components as in Figure 1.

After oxygen exposure at 375 K the C 1s spectrum in Figure 1 is dominated by the C_2 (46%) and C_3 (42%) components. Curve fitting of the corresponding Ir $4f_{7/2}$ spectrum reveals the following relative coverages: $\theta_0 =$ 0.10 ML, $\theta_1 = 0.83$ ML, and $\theta_2 = 0.08$ ML, giving $\theta_{Ox} =$ 0.33 ML. As before we can calculate the average O-coverage below graphene at 375 K as (0.33 ML − 0.225 ML)/0.5 = 0.21 ML. This oxygen coverage suggests that oxygen intercalates graphene fully at 375 K and the average O-coverage is similar to the one of a p(2 × 2) structure. We therefore tentatively assign the C_2 component to a p(2 × 2) structure formed below graphene.

By exposing a 0.5 ML graphene film to oxygen at 380 K the intercalation process can be followed in real time by monitoring the C 1s region. Here, we exposed the sample to 1 × 10^{-7} mbar O_2, the O_2 pressure was stabilized at 300 K, and within 4 min the sample was heated to 380 K where it was kept during the remaining oxygen exposure time.

Curve fitting of the C 1s spectra with the same components as described above gives the evolution of the components and the corresponding oxygen phases, as seen in Figure 3 (for a movie of the C 1s spectra during oxygen exposure see Supporting Information). Initially the C_1 component grows, indicating a dilute oxygen phase growing underneath the

graphene. As the C_1 component reaches its maximum, the C_2 component starts to increase due to the formation of the p(2 × 2)-O structure. Finally, the growth of the C_3 initiates once the C_2 component reaches its maximum value.

The intercalation process followed in real time shows the subsequent formation of more and more dense oxygen phases below the graphene flakes. This picture is fully consistent with what is shown in Figure 1, where the same C 1s components are seen to appear at increasing temperatures as more oxygen is able to intercalate the graphene flakes.

Altogether, our observations suggests the following picture of oxygen adsorption on Ir(111) supported graphene. Intercalation requires the presence of bare iridium and therefore no C 1s core level shift is observed on perfectly closed 1 ML graphene films. The absence of any C 1s CLS establishes, that graphene can be grown as a hole-free membrane, impenetrable to molecular oxygen. On the sample with the partial 0.5 ML graphene coverage O_2 dissociation takes place on bare Ir(111) patches, where a p(2 × 1)-O adlayer is formed. At 300 K this adlayer remains and no oxygen penetrates under the graphene flakes. Increasing the temperature up to 355 K causes more and more graphene flakes to become intercalated by a dilute oxygen adatom gas. At higher temperatures around 375 K graphene flakes become intercalated by dense oxygen p(2 × 2)-O and p(2 × 1)-O adlayers. For $T \geq 400$ K a defective oxygen p(2 × 1)-O adlayer is present on the entire Ir(111) surface, be it pristine or covered by graphene flakes.

Thus the XPS fingerprints of the intercalated p(2 × 1)-O phase have been determined for the respective core level to be a C 1s CLS of −0.45 to 283.64 eV and a narrowing of the peak in C 1s, disappearance of the Ir_0 component and appearance of Ir_1 and Ir_2 components in Ir $4f_{7/2}$ and an O 1s peak positioned at 529.9 eV, corresponding to oxygen on Ir(111). Armed with these fingerprint values of O-intercalated graphene we revisit the previous XPS-studies of atomic oxygen adsorption on graphene/Ir(111). In the recent work by Vinogradov *et al.*[14] the authors observed and assigned an O 1s peak at 529.0 eV to intercalated oxygen after it was exposed to atomic oxygen at room temperature. The authors tentatively explained that the −1 eV CLS with respect to oxygen adsorption on clean Ir(111) is caused by the overlaying graphene film. More recently, Larciprete *et al.*[15] questioned this assignment (528.8 eV in the work by Larciprete *et al.*) based on the oxygen peak desorption behavior. Instead they suggested that the ∼529 eV component should be assigned to O-atoms adsorbed in the moiré regions closer to the metal substrate in analogy with the H adsorbates. Since we measure an O 1s binding energy of 529.9 eV for intercalated oxygen, identical to oxygen on clean Ir(111), we can rule out that the O 1s feature at ∼529 eV observed after atomic oxygen exposure can originate from intercalated oxygen. Furthermore, we find that intercalation of oxygen is reflected by a −0.45 eV CLS of the C 1s peak of graphene. None of the studies by Vinogradov *et al.* or Larciprete *et al.* found C 1s components with a negative shift that occurred simultaneously with the 529 eV peak. We therefore agree with Larciprete *et al.* and conclude that the O 1s component at 529 eV should be assigned to something else than intercalated oxygen. However, at higher oxygen exposures Larciprete *et al.* observe a C 1s component at 283.6 eV shifted −0.5 eV with respect to their C 1s binding energy for pristine graphene. This peak is according to the authors assigned to carbon vacancies. In the corresponding O 1s spectrum the authors observe a new component at 530.0 eV, which they assign to double bonded C═O. A shift of −0.5 eV in C 1s spectrum and an O 1s peak position 530 eV is almost identical to what we observe for intercalated oxygen. We, therefore, suspect that a small amount of intercalated oxygen is responsible for the 283.6 eV C 1s component and 530.0 eV O 1s components in the work of Larciprete *et al.*

To gain additional insight into the proposed oxygen intercalation picture we performed STM investigations. Figure 4a displays Ir(111) covered with 0.5 ML graphene after oxygen exposure at 355 K. As visualized by the schematic sketch of Figure 4b the topography in Figure 4a has four Ir substrate levels separated by monatomic steps. The step edges partially act as boundaries of the graphene flakes, but they also grow over the steps. The Ir areas free of graphene are covered by atomic oxygen in the (2 × 1) structure and have a noisy appearance in Figure 4a. The graphene covered areas are rather smooth, but display a moiré of graphene with the underlying Ir(111) substrate with a periodicity of 2.53 nm and a corrugation of 0.45 Å. The moiré is well visible in the contrast enhanced box in the upper right corner of Figure 4a. Within the graphene covered area four small islands with an apparent height of 0.9 Å are present [striped red-yellow in Figure 4b], close to substrate steps, three of them next to each other. The area fraction of these islands is below 5% of the graphene area, consistent with the small intensity of the C_2 and C_3 components for the 355 K C 1s spectrum in Figure 1. We propose that these small islands represent a dense phase of intercalated oxygen underneath graphene, either in the (2 × 2) or in the (2 × 1) structure, as visualized in the cross section shown in Figure 4c which is taken along the blue line in Figure 4a. We assume the other graphene covered areas to be not intercalated or to only possess an oxygen lattice gas intercalation phase consistent with the observation of the C_{Ir} and C_1 components in the XP-spectra.

Additional evidence for this assignment comes from Pt deposition experiments. To understand their

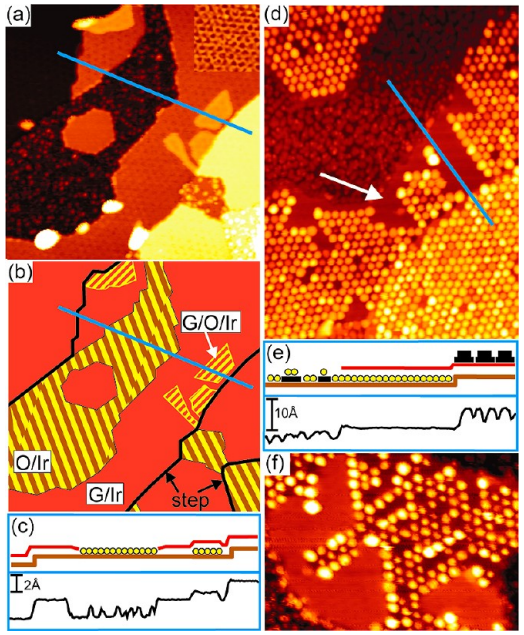

Figure 4. (a) STM topograph of Ir(111) covered with 0.5 ML graphene after exposure to 750 L of O_2 at 355 K. In the contrast enhanced box in the upper right corner the moiré is visible. Image size 70 nm × 70 nm. (b) Schematic representation of panel a in top view. Full black line, Ir step edge; red, graphene on Ir(111) (G/Ir in the schematics); striped brown-yellow, Ir with adsorbed O (O/Ir); striped red-yellow, graphene with intercalated oxygen(G/O/Ir). (c) (Upper panel) schematic cross section along blue line as indicated in panels a and b: brown, Ir; red, graphene; yellow dots, adsorbed oxygen atoms. (Lower panel) STM height profile along blue line in panel a. (d) STM topograph of the same preparation as in panel a, but with additional deposition of 0.3 ML Pt at 300 K. The white arrow indicates an area where no cluster array was formed on graphene. Image size 70 nm × 95 nm. (e) Upper panel: schematic cross section along the blue line in panel d: black, Pt; other colors as in panel c. Lower panel: height profile along blue line in panel d. (f) STM topograph after similar preparation as in panel d, but less Pt was used for postdeposition. Image size 50 nm × 35 nm.

outcome we first review a few previous results related to graphene on Ir(111). The incommensurate moiré unit mesh consists of (10.32 × 10.32) graphene unit cells resting on (9.32 × 9.32) Ir atoms.[17] Owing to the varying lateral positioning of the C-atoms with respect to Ir, we identify three high symmetry regions in each moiré unit cell: in an atop area (fcc- and hcp area) we find underneath the center of a hexagonal carbon ring an atop Ir site (regular hollow or fcc-site and faulted hollow or hcp-site). In ref 25 it was found that the binding of graphene to Ir is dominated by physisorption with an average binding energy of E_b = 50 meV per C-atom and an average height of 3.38 Å. However, this binding is modulated, with weak chemical bonds in the hcp- and fcc areas and chemical repulsion in the atop areas. The weak bonds are formed through weak hybridization of Ir($5d_{3z^2-r^2}$) orbitals with C($2p_z$) orbitals, where C atoms of graphene and Ir substrate atoms sit in juxtaposition. In the chemically repelled atop areas (with no C atoms in juxtaposition to Ir atoms) graphene has a larger distance from the substrate resulting in a graphene corrugation of about 0.4 Å. Upon Pt deposition on graphene, the cooperative attack of substrate Ir($5d_{3z^2-r^2}$) orbitals and deposit Pt($5d_{3z^2-r^2}$) orbitals on the graphene π-electronic system causes graphene to locally hybridize from sp^2 to sp^3 in the hcp areas, implying chemical bond formation between Ir−C and C−Pt and thus cluster binding.[26] It is evident that a saturated intercalated oxygen adlayer between Ir and graphene will prevent Ir−C chemical bond formation and thereby inhibit graphene rehybridization and thus impede cluster pinning. Therefore, upon Pt deposition, no Pt cluster arrays are expected to form in graphene areas with dense intercalated oxygen phases underneath.

Figure 4d shows the oxygen exposed 0.5 ML graphene sample discussed above after additional deposition of 0.3 ML Pt at room temperature. More than 95% of the graphene covered area displays a well ordered Pt cluster array, consistent with the absence of a dense oxygen phase corresponding to the C_2 or C_3 components in Figure 1. We have to conclude that the presence of a dilute oxygen adatom gas underneath the graphene flakes (the C_1 component) does not impede cluster growth. It is plausible that the oxygen adatoms of the dilute phase linked to the C_1 component are sitting preferentially in atop areas underneath the graphene. There, graphene is most distant from the Ir(111) substrate and not even weak bonds between the two exist. Thus, no (or the smallest) energy penalty has to be paid for intercalating oxygen under the atop areas. Upon Pt deposition, this location of the O adatoms does not disturb the local graphene rehybridization and cluster binding, as it takes place in the hcp areas where O is absent. Small patches of graphene without an ordered Pt cluster array are also observed in Figure 4d. These patches are assigned to the areas where a dense phase of intercalated oxygen is present. Our interpretation of the morphology is visualized by the schematic cross section displayed in Figure 4e, which is taken along the blue line in Figure 4d. Final evidence for our assignment comes from Figure 4f. It represents a surface morphology after a similar treatment as in Figure 4c, but with less Pt deposited. As a result the clusters are smaller and it is easier to observe the graphene substrate between the clusters. An analysis of Figure 4f reveals that the graphene level is 0.9 Å higher in the cluster-free region as compared to the graphene substrate with clusters, thereby confirming our interpretation. We note that to distinguish between intercalated and nonintercalated graphene areas on Ru, Ru postdeposition has been used, though resulting in a weaker contrast and probably not related to graphene rehybridization.[27]

Next we give the real space view of the 400 K C 1s spectrum shown in Figure 1, that is, after exposing an 0.5 ML graphene covered Ir(111) sample to O_2 at 400 K. Figure 5a shows the corresponding STM topograph.

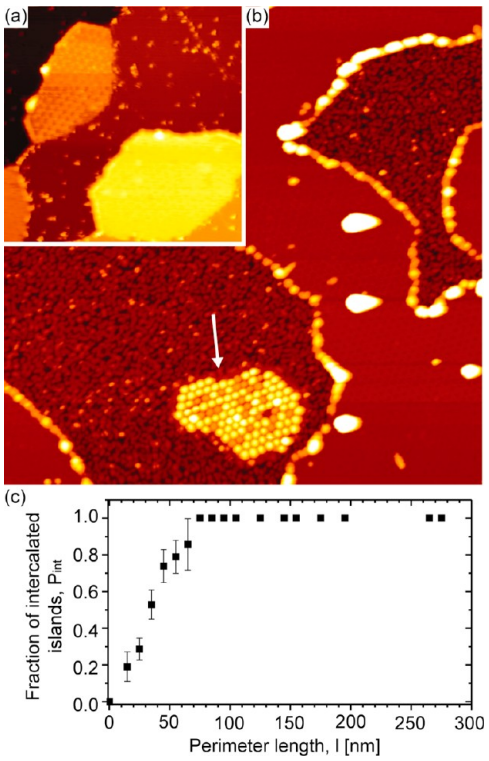

Figure 5. (a) STM topograph of Ir(111) covered with 0.5 ML graphene after exposure to 750 L of O_2 at 400 K. Image size 70 nm × 70 nm. (b) STM topograph after same preparation as in panel a, but with additional deposition of 0.3 ML Pt at 300 K. The arrow indicates a small graphene flake with Pt cluster array (see text). Image size 140 nm × 140 nm (c) Probability P_{int} for a flake to be intercalated at 400 K by a p(2 × 1)-O adlayer as a function of flake perimeter length *l* (see text). The confidence level represented by the error bars is 66%. No errors are given for less than seven perimeter lengths in a bin.

The graphene flakes in the lower part of the topograph display no visible moiré contrast. However, the graphene flake in the upper image part attached to an ascending step displays clear moiré contrast. After oxygen exposure at 400 K such flakes with clear moiré contrast are rare in the overall topography. We conclude that the nature of these flakes must be different. An unambiguous interpretation is again possible with the help of Pt deposition. Figure 5b shows the sample after an additional 0.3 ML Pt deposited at 300 K. Except for a small flake indicated by an arrow in the lower part of Figure 5b, no cluster arrays are formed on the graphene flakes. The Pt agglomerates to a few large clusters which are randomly distributed on the flakes. Also decoration of the graphene flake edges by Pt is apparent. This finding is consistent with our conclusions based on the XPS data, namely that at 400 K the vast majority of the graphene area has a dense p(2 × 1)-O adlayer intercalated, corresponding to the C_3 component.

Analysis of a large number of STM images of oxygen exposed graphene reveals the following features. (i) At 355 K the phase boundaries between dense and dilute intercalation areas are sharp. (ii) At 355 K the phase boundaries largely follow the moiré structure. Densely intercalated areas are mostly quantized laterally in units of the moiré cell. (iii) At 355 K densely intercalated areas are typically attached to substrate steps covered by graphene, mostly close to a location where a graphene flake crosses a substrate step. The intercalated areas are only found under graphene flakes grown over a step edge. (iv) At 400 K graphene flakes are either *fully* intercalated with a p(2 × 1)-O intercalation phase or only with a dilute adatom gas. Not a single phase boundary within a graphene flake is observed out of a sample of more than 10^3 graphene flakes. (v) At 400 K few graphene flakes without a p(2 × 1)-O intercalation layer remain. They are all among the smallest ones. (vi) At 400 K the apparent moiré corrugation of intercalated flakes with ≈0.1 Å is substantially lower than the one of nonintercalated ones with ≈0.45 Å.

The sharpness of the phase boundaries at 355 K (i) and their relation to the moiré (ii) most likely trace back to the binding energy inhomogeneity of graphene on Ir(111) mentioned above. When a dense oxygen adlayer is formed underneath graphene, the more strongly bound hcp and fcc areas need to be delaminated from the graphene. In consequence they form an obstacle for the expansion of the intercalated dense O phase and sharp phase boundaries are formed between the oxygen adatom lattice gas (not requiring delamination, as O is located primarily in the atop areas) and the O-islands in the p(2 × 2) or p(2 × 1) phase. Findings iii−v tell us about the pathway of intercalation. The formation of a dense phase of atomic oxygen on the Ir(111) surface under the graphene flake encompasses two basic steps: (a) delamination of the graphene flake starting at its edge and (b) oxygen transport under the flake through surface diffusion to establish a dense oxygen intercalation phase. The fact that after oxygen exposure at 400 K all large graphene flakes are fully intercalated with a p(2 × 1)-O oxygen phase, while only a few small graphene flakes are not delaminated, tells us immediately that at this temperature the formation of the p(2 × 1)-O intercalation layer is not diffusion limited but boundary limited. Diffusion limitation would make it difficult for the phase boundary to reach the center of large graphene flakes (which is not the case), while boundary limitation says that the key process is to propagate the p(2 × 1)-O ad-layer on the Ir(111) terrace through the flake edge underneath the graphene flake, that is, to pass the flake edge. Moreover, the absence of phase boundaries underneath the graphene flakes tells that the delamination of a flake at 400 K must be considered as a single, fast event.

In Figure 5c we plot the observed fraction P_{int} of p(2 × 1)-O intercalated and delaminated graphene flakes confined to a single Ir terrace as a function of the flake perimeter length *l*. Graphene flakes that are not confined to a single Ir terrace, that is, that grow across a substrate step, are not included in the statistics (see

below). This implies that our analysis is not valid for a percolated graphene film with holes or even for the perfectly closed layer. For the analysis we evaluated I for a total of 177 graphene flakes. It is obvious from the analysis that P_{int} is a strongly increasing function of I. P_{int} reaches unity for flakes with a perimeter of 80 nm and beyond. Assuming that the propagation of the p(2 × 1)-O adlayer beyond the flake edge is a process with a small probability that is attempted independently and randomly along the flake edge yields an initial linear increase of P_{int} with I, which has to level off, when approaching $P_{int} = 1$, as observed.

Why is it difficult for oxygen to propagate the p(2 × 1)-O adlayer underneath the graphene flake edge and what is the nature of this unlocking-process? As shown by Lacovig *et al.*,[28] the graphene flake edge dangling bonds tend to bind to the Ir substrate. Therefore the flakes bend down at the edge, as indicated in the schematics of Figure 4c. While single oxygen adsorbates—forming an oxygen adatom lattice gas—may diffuse underneath the graphene flake into the unbound atop areas without lifting the flake edge and the flake itself to a significant extent, the formation of a dense oxygen adlayer requires the entire unbinding of graphene. Unbinding of a graphene moiré unit cell at the flake edge requires unbinding of the flake edge bonds plus unbinding of the graphene moiré unit cell adjacent to the edge. In contrast, the unbinding of a moiré unit cell within the flake requires no additional unbinding of edge bonds. The force required for the unbinding of a moiré unit cell at the flake edge is therefore evidently larger than the one for unbinding a cell in the interior of the flake. This explains why even very large flakes are delaminated rapidly, once the phase boundary passed the flake edge. For graphene flakes confined to a single Ir(111) substrate terrace, unbinding of the graphene flake edge may therefore be considered as the rate limiting step in intercalation at 400 K.

The additional question arises, how the adsorbed oxygen on the terrace may exert the unbinding force at the graphene edge. To answer this question it is of key importance to note that close to saturation the adsorption energy of oxygen on Ir(111) decreases considerably because of repulsive adsorbate−adsorbate interactions.[20,29] Consider now the saturated p(2 × 1)-O adlayer at the graphene flake edge. The adlayer exerts a one-dimensional pressure (force per unit length) on the graphene flake edge, as a local expansion of the adlayer into the space underneath the flake will increase the binding energy (larger adsorbate separation). Through local fluctuations in coverage (and thus force) at some point along the flake edge, unbinding will occur. The probability for an unbinding event at the flake edge will be proportional to the perimeter of the edge, as observed. It is followed by rapid expansion of the adlayer underneath the flakes. The fixed chemical potential of the gas phase will replenish oxygen on the Ir(111) terrace until eventually the p(2 × 1)-O adlayer is established on the entire surface, on the bare Ir terrace and under the graphene flakes. These considerations also explain why delamination does not start in the center of a graphene flake: although some oxygen is present there, its concentration is low and thus so is the force that can be exerted to unbind. Our experiments related to the energetics of intercalation presented in what follows (Figure 7 and 8 with discussion) are fully consistent with the above picture. However, we are unable to specify the unbinding process in terms of the atomistic reaction pathways and potential energy barriers. To this end density functional theory calculations and more detailed experiments are highly desirable.

In the description of Figure 5b we noted that the Pt deposition causes an edge decoration of flakes delaminated by an intercalated (2 × 1) adsorbate layer. This edge decoration with Pt-clusters is absent for small flakes that have not been delaminated and which display a regular cluster array. In the picture proposed above, the Pt edge decoration is expected: After unbinding the graphene edges from the substrate they are likely to be reactive and will consequently act as heterogeneous nucleation sites for Pt.

While our concept of edge unbinding as a rate limiting step for the formation of dense oxygen adlayers underneath graphene flakes explains all of our observations convincingly, it is worthwhile to consider an alternative scenario based on the oxygen intercalation experiments on Ru(0001). Sutter *et al.*[10] and Starodub *et al.*[11] observed that once the oxygen exposure to Ru(0001) stops, O disappears from under graphene flakes already at 550 K and close to the edge of a graphene flake deintercalation takes place first. An alternative interpretation of the Pt decoration experiment of Figure 5b would then be that for the small graphene flakes the oxygen has leaked out by the time of the STM analysis, while the edges of the large flakes would, after some oxygen loss at the edges, rebind to the Ir, keeping the O trapped inside. Instead of hindered intercalation under small flakes, our Pt postdeposition experiments would then visualize the more rapid deintercalation of oxygen from under small flakes. The edge decoration of the large flakes would then not be the consequence of reactive flake edges but of graphene rebound to the substrate. This scenario based on oxygen intercalation under graphene on Ru(0001) experiments does not apply for the following two reasons.

(1) Oxygen adsorption on Ir(111) is a true 2D adsorption system. Thus, once the sample is saturated with oxygen in a p(2 × 1)-adlayer only combustion with graphene ($T > 550$ K) or oxygen desorption ($T > 750$ K) might lower the surface coverage. Both processes possess onset temperatures well above 400 K and are thus irrelevant. As the oxygen adlayer was saturated in a pressure of 1×10^{-5} mbar, an unreasonable amount

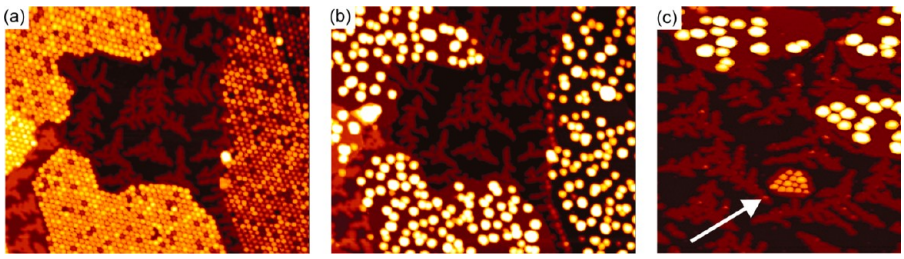

Figure 6. STM topographs of 0.3 ML Pt deposited at 300 K on 0.5 ML graphene/Ir(111). (a) Imaged at 400 K before oxygen exposure. (b) Imaged at 400 K during oxygen exposure to 1×10^{-7} mbar of O_2 after 1930 s (145 L). (c) STM topograph of 0.3 ML Pt deposited at 300 K on 0.2 ML graphene/Ir(111) after exposure to 750 L of O_2. Arrow indicates nondelaminated graphene flake (see text). Image sizes are (a and b) 120 nm × 100 nm and (c) 70 nm × 70 nm.

of energy would be necessary to compress the saturated O adlayer in consequence of deintercalation. There is no space to go for the oxygen from under a flake; all surrounding Ir terraces are saturated with oxygen.

(2) A striking proof that the above scenario fails is contained in Figure 6. Figure 6a displays Pt-clusters grown on the graphene flakes *before* oxygen exposure. Upon oxygen exposure at 400 K with an oxygen pressure of 1×10^{-7} mbar the Pt cluster arrays of *large* graphene flakes suddenly disorder after an exposure to 6 L. The final state is shown in Figure 6b after 145 L (for an extended image sequence see Figure S6 in the Supporting Information). The clusters become mobile and coalesce to form large clusters, which are less dense and irregularly distributed on the flakes. Figure 6c displays a small and several larger graphene flakes after a similar experiment. While the large graphene flakes display detached clusters, the array on the small graphene flake indicated by the white arrow is still intact. Our interpretation is as follows: Upon O_2 exposure oxygen adsorbs on the Ir(111) terrace and intercalates under the graphene flakes in the very same way, as if the clusters would not be present. Upon formation of a dense oxygen intercalation layer, graphene becomes detached from the Ir(111) substrate and the local sp^3 hybridization is lifted.

In consequence the clusters are unbound, become mobile, and aggregate to larger entities which eventually come to rest. Our observations imply that the increased delamination energy due to cluster binding is not a substantial hindrance for the formation of a dense intercalation layer. Our observations also imply that where the cluster array was not destroyed, as for the small graphene flake in the lower part of Figure 6c, no dense oxygen layer intercalated. Thereby, the scenario developed above on the basis of observations related to oxygen intercalation under graphene on Ru(0001) is refuted.

Coming back to our list of observations extracted from the STM images, observation iii at 355 K indicates that graphene flakes extending over several terraces are somewhat special. At this lower temperature, densely intercalated areas are typically attached to substrate steps covered by graphene, mostly close to a location where a graphene flake crosses a substrate step (compare Figure 4a; additional examples are visible in the large scale topograph in Figure S7 of the Supporting Information). Our interpretation is as follows: Where a graphene flake grows over a substrate step a larger graphene–Ir separation is found.[30] Therefore at these locations oxygen more easily unbinds the graphene locally and diffuses in under the flake along the more spacious tunnel formed through the graphene flake and the ascending step. Occasionally oxygen is able to unbind a small area adjacent to the tunnel and spreads away from the step forming a dense intercalation patch. Note that one of the four small intercalation patches in Figure 4a has a small gap to the substrate step. We observe that the shape of intercalation patches may fluctuate while imaging. Therefore small intercalation patches may also be pinched off the substrate step or a patch connected to it. We emphasize that single intercalation patches are not found in the central area of a substrate terrace covered by graphene (compare Figure S7). As at 355 K we never observe entire intercalated flakes, we conclude that at this low temperature the delamination of graphene within the flake is an effective barrier for the spreading of the dense oxygen intercalation phase.

We note that we are unable to identify the rate limiting step for the formation of the oxygen adatom lattice gas under graphene flakes with certainty. We assume that it is just the onset of the surface diffusion of atomic oxygen on Ir(111) that enables its formation. At least the increase of the p(2 × 1)-O domain size from room temperature to 400 K as seen by STM is consistent with this assumption.

The substantially reduced corrugation of the moiré (vi) after delamination of the graphene through intercalated oxygen is fully consistent with our XPS experiments. When we discussed Figure 1, we noted that the reduced GFWHM of the new C_3 component representing graphene floating on intercalated oxygen indicates a reduced height modulation. This is exactly what we observe in STM.

Now we address the question whether atomic oxygen, once formed on the bare Ir(111) terraces, is more

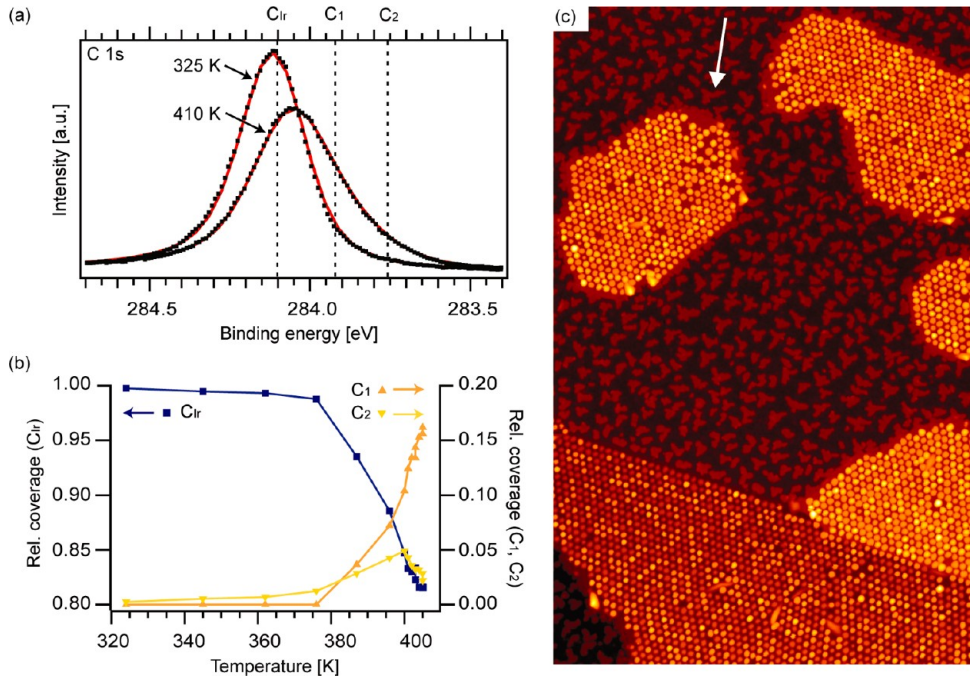

Figure 7. The 0.5 ML graphene/Ir(111) was exposed to 750 L of O_2 at 300 K and subsequently heated to 410 K. The (a) first (325 K) and last (410 K) C 1s spectra taken during heating are displayed. The experimental data are shown as dots and the fits as red lines. (b) Partial coverages of the fit components C_{Ir}, C_1, and C_2 for the spectra are plotted as a function of temperature. (c) STM topograph taken after the experiment visualized in panels a and b, but with additional deposition of 0.3 ML Pt at 300 K. Image size is 140 nm ×220 nm.

strongly bound underneath the graphene flakes than on the bare Ir. We already demonstrated that no covalent bonds are formed between oxygen and graphene (absence of XPS signatures for ethers and epoxy groups). However, if intercalated oxygen would cause a strong charge transfer of graphene from electrostatic interaction, an enhanced binding energy of oxygen underneath graphene could result.

In a first experiment we exposed 0.5 ML graphene on Ir(111) to 750 L O_2 at room temperature. As described above, intercalation is absent and the p(2 × 1)-O structure is present only on the bare Ir(111) patches at this temperature. Subsequently, we heated the sample to 410 K in the *absence* of an applied oxygen pressure. The C 1s region was monitored during heating. In Figure 7a the first and the last C 1s spectrum of the experiment are displayed. Figure 7b shows the result from curve fitting of the C 1s spectra taken during the heating. The components are the same as in Figure 1. Initially, only the C_{Ir} component is present in Figure 7a. Upon heating the C_{Ir} component is seen to decrease, whereas the C_1 component increases. A very small C_2 component is also seen in the temperature interval 380−410 K. After heating to 410 K a visible shift toward lower binding energy is observed and the spectrum can be deconvoluted by the C_{Ir} (82%), C_1 (16%) and C_2 (2%) components.

The observation of the C_1 component tells that a dilute oxygen lattice gas formed below many graphene flakes when the surface is heated to 410 K. The absence of the C_3 component implies the absence of a p(2 × 1)-O adlayer below graphene. The marginal size of the C_2 component implies an only marginal size of p(2 × 2)-O adlayers below graphene. Oxygen combustion with graphene during the heating can be excluded as we observe that above 550 K. Consistent with these XPS findings regular cluster arrays form on the graphene flakes when Pt is deposited afterward (compare Figure 7c), except in a few locations at the edges of graphene flakes. These disturbed areas (see arrow in Figure 7c) may be linked to the small magnitude of the C_2 component.

Without applied oxygen pressure no dense oxygen adlayer forms underneath the graphene flake. The outcome of this experiment is consistent with our considerations described above. The dilute adatom gas forms underneath, as this enables lowering the concentration of oxygen on the terrace and thereby increasing the average oxygen binding energy to Ir(111).[20] As the initially saturated p(2 × 1)-O adlayer on the Ir terraces decreases in oxygen density, the force exerted by it on the graphene flakes will rapidly drop to an extent that graphene delamination does not take place, or only to a marginal extent. While this experiment is fully consistent with the absence of an energetic preference for oxygen to reside underneath graphene, it does not prove its absence.

In a second experiment we titrated intercalated oxygen with CO, which can be seen as the reverse experiment of oxygen intercalation. Initially, a surface

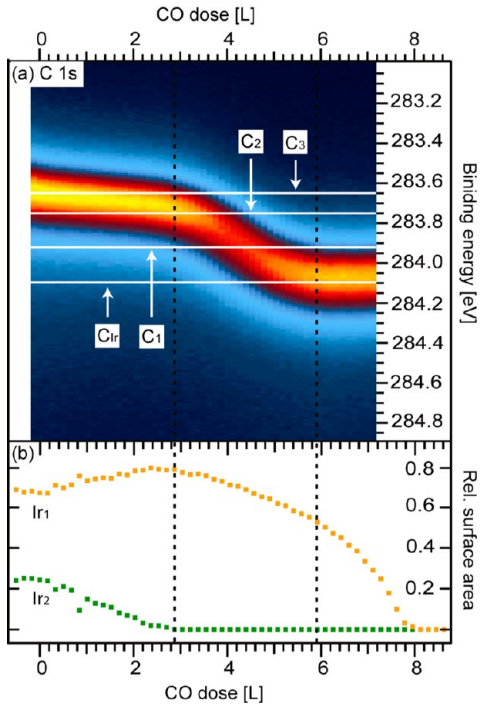

Figure 8. The 0.5 ML graphene/Ir(111) was exposed to 1 × 10^{-5} mbar of O_2 for 100 s at 410 K. After oxygen intercalation the sample was heated to 490 K and exposed to 5 × 10^{-9} mbar of CO. In panel a the development of the C 1s peak upon CO exposure, from the initial oxygen intercalated position to the position of pristine graphene/Ir(111) is seen, and in in panel b the relative surface intensity of the oxygen induced Ir surface components is displayed. Both the Ir $4f_{7/2}$ and C 1s core levels were followed in real time.

covered with 0.5 ML graphene was exposed to 750 L of O_2 at 410 K to obtain full intercalation. After oxygen intercalation the sample was heated to 490 K and exposed to 5 × 10^{-9} mbar of CO. The titration was followed in real time by acquisition of the C 1s region and the Ir 4f region. We note that a temperature of 490 K is too low for graphene etching or oxygen desorption. Details about the etching of graphene will be discussed in a forthcoming publication.

The C 1s spectra are shown in Figure 8a as an image plot. The CO dose is given on the *x*-axis, and the binding energy is given on the *y*-axis, while the intensity is shown with color code. The corresponding Ir $4f_{7/2}$ spectra were fitted with the same components as in Figure 2 and the resulting peak areas of the surface components are shown in Figure 8b. Initially, a small negative CLS in the C 1s region develops, simultaneously with the Ir_2 component decrease. Once the Ir_2 component reached zero the C 1s CLS matches extremely well with the fingerprint of graphene intercalated by a p(2 × 2)-O structure, that is, with the position of the C_2 component (see Figure 8a). After the Ir_2 component disappeared the Ir_1 component starts to decrease and the C 1s CLS decreases rapidly. This implies that oxygen deintercalates to an extent that graphene adheres again to Ir(111), that is, relaminates Ir(111). Once, the C 1s peak reaches the C_{Ir} peak position, the coverage of Ir_1 atoms has dropped to approximately half of the coverage as compared to the measured coverage of the p(2 × 2)-O structure at the dashed line at 3 L CO. We conclude that at this point of the titration we have the p(2 × 2)-O structure on the bare Ir and fully laminated graphene flakes. This is a key finding: despite the fact that the titration reaction removes oxygen only from the bare Ir terraces (CO cannot penetrate under graphene at the low pressure applied[31]), at this point the oxygen concentration on the bare Ir terraces is *larger* than underneath the graphene flakes. Apparently graphene expels oxygen. This finding can only be understood, if oxygen energetically prefers to reside on the bare Ir rather than underneath graphene flakes. Thus, the CO titration experiment directly proves that O-intercalation weakens the binding of graphene to the substrate, since an overall binding energy gain of graphene bonded to the Ir(111) substrate is the only way to explain the energetic preference of oxygen on the bare Ir(111). Further, titration diminishes the remaining Ir_1 component due to loss of oxygen from the terraces and eventually we are left with clean Ir(111) partly covered by nonintercalated graphene.

CONCLUSIONS

Our studies show that under an applied oxygen pressure no intercalation under a closed graphene layer takes place. Graphene on Ir(111) can be grown as an impenetrable hole-free membrane. In contrast, for 0.5 ML graphene coverage a temperature-dependent intercalation behavior is observed. Up to 300 K no intercalation takes place. With increasing temperature more and more flakes are intercalated by a dilute oxygen adatom lattice gas. This gas coexists with the dense p(2 × 1)-O adlayer on the bare Ir(111) terraces. Its formation is not associated with graphene flake delamination. At 355 K first small patches of intercalated dense oxygen adlayer are observed, coexisting with the intercalated oxygen adatom lattice gas. Oxygen adlayer patches are found adjacent to substrate edges covered by graphene resulting from oxygen indiffusion along the spacious tunnel formed by the substrate step and the graphene flake. At 400 K all graphene flakes with a perimeter length larger than 80 nm are intercalated by a p(2 × 1)-O adsorbate layer. Flakes confined to a single Ir terrace and with a perimeter length below 80 nm resist intercalation through a dense oxygen adlayer the more likely the shorter their perimeter length is. The rate limiting process for delamination of such graphene flakes through intercalated oxygen is thus the unbinding of the graphene flake edges from the substrate. Once unbinding took place at a location at the flake boundary, at 400 K fast delamination and intercalation of the entire flake takes place.

With XPS and STM we determined the fingerprints of the intercalated p(2 × 1)-O phase to be the following: (i) A −0.45 eV CLS of the C 1s peak originating from C-atoms in graphene, (ii) a 15% narrowing of the C 1s peak width, (iii) a single O 1s component with BE of 529.9 eV, (iv) disappearance of the Ir surface component and appearance of Ir_1-O and $O-Ir_2-O$ components with an Ir $4f_{7/2}$ BE of 60.62 and 61.11 eV, respectively, (v) a by 0.9 Å increased height of areas or entire flakes over the one of pristine graphene, (vi) a drastically reduced apparent moiré corrugation around 0.1 Å, and (vii) the lack of a regular Pt cluster array after room temperature Pt deposition, caused by the suppression of graphene rehybridization through the intercalated oxygen. The formation of the p(2 × 1)-O structure with molecular oxygen is fundamentally different from the formation of the epoxy groups, esters, quinons, and lactones that has been reported to form upon exposure to atomic oxygen.

Intercalation of dense oxygen adlayers requires an applied oxygen pressure. It is necessary to exert and maintain the oxygen induced forces on graphene flakes to enable them to unbind from the substrate. An applied oxygen pressure not only causes delamination of pure graphene from Ir(111), but also of graphene flakes with Pt cluster arrays. In the absence of an applied oxygen pressure a p(2 × 1)-O adlayer on the bare Ir terraces relaxes by formation of an oxygen adatom lattice gas underneath graphene flakes, enabling an increase of the average binding energy per oxygen adsorbate slightly. From CO titration experiments we conclude that intercalated graphene flakes expel oxygen. Graphene energetically prefers to reside on clean Ir(111) rather than to float less bound on an intercalated dense oxygen layer.

METHODS

The XPS experiments were performed at beamline I311[32] at the MAX IV Laboratory, and scanning tunneling microscopy experiments (STM) were carried out in Cologne in an ultrahigh vacuum variable temperature STM-apparatus. The base pressure in both systems was better than 1×10^{-10} mbar.

The Ir(111) crystal was cleaned by cycles of Ar^+ (XPS) or Xe^+ (STM) sputtering at room temperature with subsequent O_2 treatment at 1200 K (1×10^{-7} mbar, 10 min), followed by vacuum annealing to above 1400 K. No subsurface Ar gas bubbles were observed with the STM and we can thus exclude that such subsurface bubbles modified the intercalation process, as Jin *et al.* reported for oxygen intercalation on graphene/Ru(0001).[33] Temperatures are measured with a chromel-alumel thermocouple spot-welded to the side of the crystal.

The growth of a partial graphene layer with 0.5 ML (0.95 ML) coverage was performed by three (10) cycles of ethylene (C_2H_4) adsorption until saturation at room temperature followed by thermal decomposition at 1400 K.[16,17] Here, 1 ML (monolayer) graphene corresponds to full coverage of the Ir(111) substrate. The resulting 0.5 ML graphene is not yet percolated and consists of flakes and coalesced flakes with a broad size distribution with CE diameters of 10−100 nm. The 0.95 ML graphene is percolated and displays in STM uncovered Ir(111) patches at distances of the order of micrometers. The perfectly closed 1 ML graphene was grown by one cycle of adsorption and thermal decomposition followed by chemical vapor deposition of ethylene ($p = 1 \times 10^{-7}$ mbar) for 2400 s at 1170 K.[34] These growth recipes yield for all graphene coverages only the well-known incommensurate (9.32 × 9.32) moiré superstructure with the dense packed rows of graphene and Ir(111) in parallel with a scatter of less than ±0.5°.[17] The quality and uniqueness of orientation of the prepared graphene and the absence of differently oriented domains was checked by low energy electron diffract (LEED) in both the STM and the XPS chamber.

In the XPS chamber the absence of CO adsorption at room temperature confirmed the closure of the 1 ML graphene layer. In the STM chamber the full coverage with graphene was directly confirmed by low magnification STM imaging all over the sample.

Oxygen exposure is conducted in an O_2 pressure of 1×10^{-5} mbar for 100 s, if not specified otherwise. The resulting dose of 750 L is more than an order of magnitude larger than what is necessary to reach saturation coverage on Ir(111).[23,24] High purity Pt was sublimated with a commercial E-beam evaporator, resulting in a typical deposition rate of 3×10^{-2} ML/s. Pt coverages are defined, such that 1 ML corresponds to the surface atomic density of Ir(111). During Pt-deposition the sample was kept at 300 K and the pressure remained in the low 10^{-10} mbar range. The Pt evaporator was calibrated in the STM chamber by determination of the fractional area of monolayer Pt-islands deposited onto clean Ir(111).

All XP-spectra were collected in normal emission with photon energies of 190 eV for Ir 4f, 390 eV for C 1s, and 650 eV for O 1s. The total energy resolution of the light and analyzer is better than 45, 60, and 200 meV for the respective core level spectra. The spectra were fitted with Doniach−Šunjić functions convoluted with Gaussians. A linear background was used for the curve fitting. The C 1s curve fitting of the stepwise O_2 dosing experiment [Figure 1 and S1] was performed simultaneously for all temperature steps. STM imaging was conducted at room temperature, if not specified otherwise. STM images were post-processed using the WSxM software.[35]

Conflict of Interest: The authors declare no competing financial interest.

Acknowledgment. Financial support from the Swedish Research Council and the Deutsche Forschungsgemeinschaft (MI581/17-2) is acknowledged. The MAX IV Laboratory personnel is acknowledged for support during measurements.

Supporting Information Available: Supporting Information available: (Figure S1) C 1s spectra after oxygen exposure of a perfectly closed 1 ML graphene layer at stepwise increasing temperatures; (Figure S2) STM topographs of a closed 1 ML graphene film (a) after oxygen exposure at 700 K and (b) after additional Pt deposition; (Figure S3) Ir 4f and C 1s spectra of an oxygen exposed 0.95 ML graphene film; (Figure S4) LEED image of oxygen exposed 0.95 ML graphene; a longer discussion of the origin of the C 1 CLS for the C_3 component; (Figure S5) O 1s spectra of oxygen exposed 0.5, 0.95, and 0 ML graphene; Movie "O2_ads.qt" that shows the time evolution of the C 1s components during oxygen intercalation (Figure 3); (Figure S6) extended image sequence of graphene supported Pt-clusters followed during oxygen intercalation; (Figure S7) large-scale STM topograph after oxygen intercalation at 355 K. This material is available free of charge *via* the Internet at http://pubs.acs.org.

REFERENCES AND NOTES

1. Riedl, C.; Coletti, C.; Iwasaki, T.; Zakharov, A. A.; Starke, U. Quasi-free-standing Epitaxial Graphene on SiC Obtained by Hydrogen Intercalation. *Phys. Rev. Lett.* **2009**, *103*, 246804.
2. Robinson, J.; Hollander, M.; LaBella, M.; Trumbull, K. A.; Cavalero, R.; Synder, D. W. Epitaxial Graphene Transistors: Enhancing Performance *via* Hydrogen Intercalation. *Nano Lett.* **2011**, *11*, 3875–3880.

3. Oida, S.; McFeely, F. R.; Hannon, J. B.; Tromp, R. M.; Copel, M.; Chen, Z.; Sun, Y.; Farmer, D. B.; Yurkas, J. Decoupling Graphene from SiC(0001) *via* Oxidation. *Phys. Rev. B* **2010**, *82*, 041411.
4. Varykhalov, A.; Sánchez-Barriga, J.; Shikin, A. M.; Biswas, C.; Vescovo, E.; Rybkin, A.; Marchenko, D.; Rader, O. Electronic and Magnetic Properties of Quasifreestanding Graphene on Ni. *Phys. Rev. Lett.* **2008**, *101*, 157601.
5. Enderlein, C.; Kim, Y. S.; Bostwick, A.; Rotenberg, E.; Horn, K. The Formation of an Energy Gap in Graphene on Ruthenium by Controlling the Interface. *New J. Phys.* **2010**, *12*, 033014.
6. Mao, J.; Huang, L.; Pan, Y.; Gao, M.; He, J.; Zhou, H.; Guo, H.; Tian, Y.; Zou, Q.; Zhang, L.; *et al*. Silicon Layer Intercalation of Centimeter-Scale, Epitaxially Grown Monolayer Graphene on Ru(0001). *Appl. Phys. Lett.* **2012**, *100*, 093101.
7. Meng, L.; Wu, R.; Zhou, H.; Li, G.; Zhang, Y.; Li, L.; Wang, Y.; Gao, H.-J. Silicon Intercalation at the Interface of Graphene and Ir(111). *Appl. Phys. Lett.* **2012**, *100*, 083101.
8. Emtsev, K. V.; Zakharov, A. A.; Coletti, C.; Forti, S.; Starke, U. Ambipolar Doping in Quasifree Epitaxial Graphene on SiC(0001) Controlled by Ge Intercalation. *Phys. Rev. B.* **2011**, *84*, 125423.
9. Gierz, I.; Suzuki, T.; Weitz, R. T.; Lee, D. S.; Krauss, B.; Riedl, C.; Starke, U.; Höchst, H.; Smet, J. H.; Ast, C. R.; *et al*. Electronic Decoupling of an Epitaxial Graphene Monolayer by Gold Intercalation. *Phys. Rev. B.* **2010**, *81*, 235408.
10. Sutter, P.; Sadowski, J. T.; Sutter, E. A. Chemistry under Cover: Tuning Metal−Graphene Interaction by Reactive Intercalation. *J. Am. Chem. Soc.* **2010**, *132*, 8175–8179.
11. Starodub, E.; Bartelt, N. C.; McCarty, K. F. Oxidation of Graphene on Metals. *J. Phys. Chem. C* **2010**, *114*, 5134–5140.
12. Herbig, C.; Kaiser, M.; Bendiab, N.; Schumacher, S.; Förster, D. F.; Coraux, J.; Meerholz, K.; Michely, T.; Busse, C. Mechanical Exfoliation of Epitaxial Graphene on Ir(111) Enabled by Br_2 Intercalation. *J. Phys.: Condens. Mater.* **2012**, *24*, 314208.
13. Zhang, H.; Fu, Q.; Cui, Y.; Tan, D.; Bao, X. Growth Mechanism of Graphene on Ru(0001) and O_2 Adsorption on the Graphene/Ru(0001) Surface. *J. Phys. Chem. C* **2009**, *113*, 8296–8301.
14. Vinogradov, N. A.; Schulte, K.; Ng, M. L.; Mikkelsen, A.; Lundgren, E.; Mårtensson, N.; Preobrajenski, A. B. Impact of Atomic Oxygen on the Structure of Graphene Formed on Ir(111) and Pt(111). *J. Phys. Chem. C* **2011**, *115*, 9568–9577.
15. Larciprete, R.; Fabris, S.; Sun, T.; Lacovig, P.; Baraldi, A.; Lizzit, S. Dual Path Mechanism in the Thermal Reduction of Graphene Oxide. *J. Am. Chem. Soc.* **2011**, *133*, 17315–17321.
16. N'Diaye, A. T.; Bleikamp, S.; Feibelman, P. J.; Michely, T. Two-Dimensional Ir Cluster Lattice on a Graphene Moiré on Ir(111). *Phys. Rev. Lett.* **2006**, *97*, 215501.
17. N'Diaye, A. T.; Coraux, J.; Plasa, T. N.; Busse, C.; Michely, T. Structure of Epitaxial Graphene on Ir(111). *New. J. Phys.* **2008**, *10*, 043033.
18. Loginova, E.; Nie, S.; Thürmer, K.; Bartelt, N. C.; McCarty, K. F. Defects of Graphene on Ir(111): Rotational Domains and Ridges. *Phys. Rev. B* **2009**, *80*, 085430.
19. Hattab, H.; N'Diaye, A. T.; Wall, D.; Jnawali, G.; Coraux, J.; Busse, C.; van Gastel, R.; Poelserna, B.; Michely, T.; Meyer zu Heringdorf; *et al.* Growth Temperature Dependent Graphene Alignment on Ir(111). *Appl. Phys. Lett.* **2011**, *98*, 141903.
20. He, Y. B.; Stierle, A.; Li, W. X.; Farkas, A.; Kasper, N.; Over, H. Oxidation of Ir(111): From O−Ir−O Trilayer to Bulk Oxide Formation. *J. Phys. Chem. C* **2008**, *112*, 11946–11953.
21. Knudsen, J.; Feibelman, P.; Gerber, T.; Grånäs, E.; Schulte, K.; Stratmann, P.; Andersen, J. N.; Michely, T. Clusters Binding to the Graphene Moiré on Ir(111): X-ray Photoemission Compared to Density Functional Calculations. *Phys. Rev. B* **2012**, *85*, 035407.
22. Ng, M. L.; Balog, R.; Hornekær, L.; Preobrajenski, A. B.; Vinogradov, N. A.; Mårtensson, N.; Schulte, K. Controlling Hydrogenation of Graphene on Transition Metals. *J. Phys. Chem. C* **2010**, *114*, 18559–18565.
23. Hagen, D. I.; Nieuwenhuys, B. E.; Rovida, G.; Samorjai, G. Low-Energy Electron Diffraction, Auger Electron Spectroscopy, and Thermal Desorption Studies of Chemisorbed CO and O_2 on the (111) and Stepped [6(111) × (l00)] Iridium Surfaces. *Surf. Sci.* **1976**, *57*, 632–650.
24. Bianchi, M.; Cassese, D.; Cavallin, A.; Comin, R.; Orlando, F.; Postregna, L.; Golfetto, E.; Lizzit, S.; Baraldi, A. Surface Core Level Shifts of Clean and Oxygen Covered Ir(111). *New J. Phys.* **2009**, *11*, 063002.
25. Busse, C.; Lazić, P.; Djemour, R.; Coraux, J.; Gerber, T.; Atodiresei, N.; Caciuc, V.; Brako, R.; N'Diaye, A. T.; Blügel, S.; *et al*. Graphene on Ir(111): Physisorption with Chemical Modulation. *Phys. Rev. Lett.* **2011**, *107*, 036101.
26. Feibelman, P. J. Pinning of Graphene to Ir(111) by Flat Ir Dots. *Phys. Rev. B* **2008**, *77*, 165419.
27. Sutter, E.; Albrecht, P.; Wang, B.; Bocquet, M.-L.; Wu, L.; Zhu, Y.; Sutter, P. Arrays of Ru Nanoclusters with Narrow Size Distribution Templated by Monolayer Graphene on Ru. *Surf. Sci.* **2011**, *605*, 1676–1684.
28. Lacovig, P.; Pozzo, M.; Alfè, D.; Vilmercati, P.; Baraldi, A.; Lizzit, S. Growth of Dome-Shaped Carbon Nanoislands on Ir(111): The Intermediate between Carbidic Clusters and Quasi-free-standing Graphene. *Phys. Rev. Lett.* **2009**, *103*, 166101.
29. Miller, S. D.; Inoğlu, N.; Kitchin, J. R. Configurational Correlations in the Coverage Dependent Adsorption Energies of Oxygen Atoms on Late Transition Metal fcc(111) Surfaces. *J. Chem. Phys.* **2011**, *134*, 104709.
30. Coraux, J.; N'Diaye, A. T.; Busse, C.; Michely, T. Structural Coherency of Graphene on Ir(111). *Nano Lett.* **2008**, *8*, 565–570.
31. Grånäs, E.; Knudsen, J.; Arman, M. A.; Gerber, T.; Andersen, J. N.; Michely, T. Unpublished work.
32. Nyholm, R.; Andersen, J. N.; Johansson, U.; Jensen, B. N.; Lindau, I. Beamline I311 at MAX-LAB: a VUV/soft X-ray Undulator Beamline for High Resolution Electron Spectroscopy. *Nucl. Instrum. Meth. A* **2001**, *467*, 520–524.
33. Jin, L.; Fu, Q.; Zhang, H.; Mu, R.; Zhang, Y.; Tan, D.; Bao, X. Tailoring the Growth of Graphene on Ru(0001) *via* Engineering of the Substrate Surface. *J. Phys. Chem. C* **2012**, *116*, 2988–2993.
34. Van Gastel, R; N'Diaye, A. T.; Wall, D; Coraux, J.; Busse, C.; Buckanie, N. M.; Meyer zu Heringsdorf, F.-J.; Horn von Hoegen, M.; Michely, T.; Poelserna, B. Selecting a Single Orientation for Millimetersized Graphene Sheets. *Appl. Phys. Lett.* **2009**, *95*, 121901.
35. Horcas, I.; Fernández, R.; Gómez-Rodriguez, J. M.; Colchero, J.; Gómez-Herrero, J.; Baro, A. M. WSXM: A Software for Scanning Probe Microscopy and a Tool for Nanotechnology. *Rev. Sci. Instrum.* **2007**, *78*, 013705.